

Kinetics of Proton Release after Flash Photolysis of 1-(2-Nitrophenyl)ethyl Sulfate (Caged Sulfate) in Aqueous Solution

Stefania Abbruzzetti,^{†‡} Silvia Sottini,^{†‡} Cristiano Viappiani,^{*†‡} and John E. T. Corrie[§]

Contribution from the Dipartimento di Fisica, Università degli Studi di Parma, Parco Area delle Scienze, 7A, 43100 Parma, Italy, Istituto Nazionale per la Fisica della Materia (INFM), Parco Area delle Scienze, 7A, 43100 Parma, Italy, and National Institute for Medical Research, The Ridgeway, Mill Hill, London NW7 1AA, United Kingdom

Received March 17, 2005; E-mail: cristiano.viappiani@fis.unipr.it

Abstract: The kinetics of proton release after laser photolysis of 1-(2-nitrophenyl)ethyl sulfate (caged sulfate) have been characterized by time-resolved absorbance and photoacoustic methods. The absorbance at ~400 nm is observed to rise with a biphasic behavior in which a prompt component (formation of the nitronic acid) is followed by a slower ($\tau \approx 63 \pm 6$ ns) phase (deprotonation of the nitronic acid). The decay of this intermediate occurs with a lifetime which is affected by the pH of the solution and the laser pulse energy. In buffered aqueous solution at pH 7, 20 °C the *aci*-nitro decay rate is 18 ± 4 s⁻¹. Protons are released to the solution with rate $(1.58 \pm 0.09) \times 10^7$ s⁻¹ at neutral pH from the nitronic acid intermediate. From the numerical analysis of the protonation kinetics of suitable pH indicators, we could estimate the pK_a of the nitronic acid as 3.69 ± 0.05 . At acidic pH, a substantial fraction of the *aci*-nitro intermediate is in the protonated form and this leads to a biphasic release of protons, with the slower phase being characterized by an apparent rate constant strongly dependent on the pH. The strongly acidic character of the final photoproduct (sulfate ion) means that there is negligible buffering of photoreleased protons.

Introduction

Flash photolysis of photoactivatable (caged) compounds is an extremely powerful method for rapid in situ generation of bioactive effectors, that are rendered inert by their attachment to a photolabile protecting group.^{1,2} The most widely used photoprotecting groups are based on 2-nitrobenzyl photochemistry. Among other caged effectors, protons are of special interest for investigations aimed at studying the response of macromolecular or cellular structures and functions to rapid changes in pH (pH jumps). Rapid proton-transfer reactions are crucial in various biological processes, including transport through ion channels, photosynthesis and protein folding.^{3,4} One approach for rapid imposition of pH jumps has been by flash photolysis of phenolic compounds, where rapid proton generation occurs by ionization of the acidic excited state.^{5,6} However, phenols suffer from a disadvantage that consists of the reversible nature

of their photochemistry, which means that the pH changes last only for a few hundred microseconds. In contrast, compounds based on 2-nitroarylcarbonyl photochemistry (e.g., 2-nitrobenzaldehydes), lead to irreversible changes in pH and enable permanent steplike pH-jumps to be imposed.^{7,8} Flash photolysis experiments indicate that the photogenerated nitronic acid intermediates of these and related 2-nitrobenzyl compounds undergo deprotonation in water at neutral pH with rates in the 10^7 – 10^8 s⁻¹ range.^{9–11} The deprotonation rate is mainly governed by the pK_a of the particular nitronic acid intermediate, with the more acidic compounds having higher dissociation rates.^{3,12,13} We have previously reported pK_a values of 2.1 ± 0.1 for the nitronic acid generated by photolysis of 2-nitrobenzaldehyde, and 2.0 ± 0.2 for the nitronic acid from 4-chloro-2-nitrobenzaldehyde. The presence of methoxy substituents at positions 4 and 5 increases the pK_a to 2.6.¹³ Thus, the nitronic acid intermediate is completely deprotonated at pH values above 3–4, depending on the compound.^{9,12,13} Transient absorption showed that the *aci*-nitro intermediate formed upon photolysis

[†] Dipartimento di Fisica, Università degli Studi di Parma, Parco Area delle Scienze.

[‡] Istituto Nazionale per la Fisica della Materia (INFM), Parco Area delle Scienze.

[§] National Institute for Medical Research.

(1) Marriotti, G., Ed. *Methods in Enzymology*; Academic Press: San Diego, 1998; Vol. 291.

(2) Pelliccioli, A. P.; Wirz, J. *Photochem. Photobiol. Sci.* **2002**, *1*, 441–458.

(3) Gutman, M.; Nachliel, E. *Biochim. Biophys. Acta* **1990**, *1015*, 391–414.

(4) Gutman, M.; Nachliel, E. *Annu. Rev. Phys. Chem.* **1997**, *48*, 329–356.

(5) Gutman, M.; Huppert, D.; Pines, E. *J. Am. Chem. Soc.* **1981**, *103*, 3709–3713.

(6) Gutman, M. In *Methods in Enzymology*; Packer, L., Ed.; Academic Press: San Diego, 1986; Vol. 127, pp 522–538.

(7) Viappiani, C.; Bonetti, G.; Carcelli, M.; Ferrari, F.; Sternieri, A. *Rev. Sci. Instrum.* **1998**, *69*, 270–276.

(8) Viappiani, C.; Abbruzzetti, S.; Small, J. R.; Libertini, L. J.; Small, E. W. *Biophys. Chem.* **1998**, *73*, 13–22.

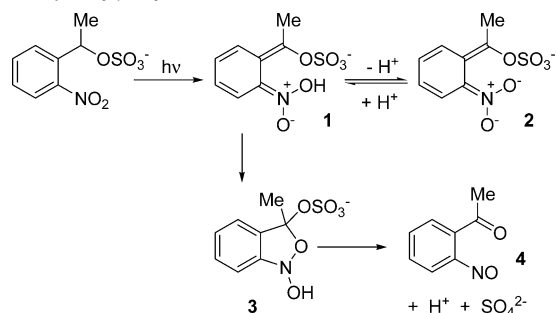
(9) McClelland, R. A.; Steenken, S. *Can. J. Chem.* **1987**, *65*, 353–356.

(10) Atherton, S. J.; Craig, B. B. *Chem. Phys. Lett.* **1986**, *127*, 7–12.

(11) Schwörer, M.; Wirz, J. *Helv. Chim. Acta* **2001**, *84*, 1441–1458.

(12) Carcelli, M.; Pelagatti, P.; Viappiani, C. *Isr. J. Chem.* **1998**, *38*, 213–221.

(13) Abbruzzetti, S.; Carcelli, M.; Rogolino, D.; Viappiani, C. *Photochem. Photobiol. Sci.* **2003**, *2*, 796–800.

Scheme 1. Proposed Reaction Mechanism for Photolysis of 1-(2-Nitrophenyl)ethyl Sulfate¹⁴

of neutral aqueous solutions of 2-nitrobenzaldehyde decays with a lifetime of 6 ± 2 ns,¹³ thus showing that the nitrosobenzoate product is formed within a few nanoseconds after photoexcitation. A possible limitation of 2-nitrobenzaldehydes is buffering of the released protons by the nitrosobenzoate photo-product.

Buffering by the released photoproduct can be avoided by another compound based on the 2-nitrobenzyl rearrangement, 1-(2-nitrophenyl)ethyl sulfate (caged sulfate; Scheme 1). This recently described compound promises to be able to achieve larger pH jumps in solution (below 3), because the low pK_a (1.92) of the sulfate product will not buffer the released proton.¹⁴ In this paper, we characterize the kinetics of proton release after nanosecond laser photolysis of caged sulfate, with particular emphasis on the effect of the initial solution pH on these kinetics.

Experimental Methods

Materials. Bromocresol green and bromophenol blue were from Aldrich. 1-(2-Nitrophenyl)ethyl sulfate (caged sulfate), 1-(2-nitrophenyl)ethyl phosphate (caged phosphate), and 1-(2-nitrophenyl)ethyl methyl phosphate (caged methyl phosphate) were synthesized as described.^{14,15} Solutions were freshly prepared before the experiments and the pH was adjusted by the addition of concentrated HCl or NaOH. Solutions used in photoacoustic experiments, and in laser flash photolysis experiments with pH indicators, were saturated with nitrogen to avoid buffering of protons by dissolved CO₂. Transient 400 nm absorption was measured for air-equilibrated solutions. The concentrations of caged sulfate, caged phosphate and caged methyl phosphate were 1 mM in the 400 nm transient absorbance experiments, while the concentration of caged sulfate was 4 mM for experiments in the presence of pH indicators. These concentrations correspond to absorbances at 355 nm (laser wavelength) of 0.1 and 0.4 respectively across the 0.2 cm laser light path through the optical cuvette (see below). The concentrations of bromocresol green and bromophenol blue were 7.2 μ M and 4.1 μ M, respectively. The concentration of caged sulfate in the photoacoustic experiments was 1 mM, corresponding to absorbance at 355 nm of 0.5 across the 1 cm laser light path. Absorbance spectra of the caged sulfate and indicators are shown as Supporting Information.

Time-Resolved Photoacoustics. Photoexcitation was achieved by the third harmonic ($\lambda = 355$ nm) of a nanosecond, Q-switched Nd:YAG laser (Surelite II – 10, Continuum).¹⁶ The unfocused beam was attenuated and shaped by a slit (280 μ m width) positioned near the cuvette. The pressure wave induced in the solution was detected by a

PZT piezoelectric transducer (Panametrics V-103). The signal was then amplified (60 dB) and recorded by a digitizing oscilloscope (LeCroy 9450A) operated at 2.5 ns/channel. A quartz cuvette was mounted inside a temperature controlled sample holder (Quantum Northwest, Inc. TASC 300) and degassed with nitrogen. Data acquisition and analysis were performed by means of dedicated software (Sound Acquisition and Sound Analysis, Quantum Northwest, Inc.). Twelve laser shots were averaged to generate each sample waveform and 100 laser shots were averaged to generate each reference waveform.

Laser Flash Photolysis. Transient absorption was measured with two different nanosecond laser flash photolysis setups. In both cases the photolysis laser was the same as used for the photoacoustic measurements. In the first setup, used for measurement of the transient 400 nm absorbance, the monitoring beam was the cw output of a 150 W Xe arc lamp (Thermo Oriel). A fast mechanical shutter (Uniblitz) was placed before the quartz cuvette (0.2 \times 1 cm) to protect the sample from undesired photolysis by the intense white light beam. The pump beam, entered the cuvette at 90° to the monitoring beam and was shaped ($\sim 1 \times 1$ cm) so as to illuminate the whole filled volume of the cuvette (200 μ L). The optical path length of the pump beam was 0.2 cm, while that of the probe beam was 1 cm. The shutter was opened 10 ms before the laser flash and was closed after the end of the data acquisition time window. The cuvette was held in a temperature-controlled sample holder (FLASH 100, Quantum Northwest, Inc.). The transmitted intensity of the cw beam was monitored by a preamplified (Avtech AV149) avalanche silicon photodiode (Hamamatsu, S2382). A 0.25 m monochromator/spectrograph (Oriel, MS257) was placed before the photodiode to select the monitoring wavelength. To remove stray light from the pump laser and increase time resolution, a custom-made dichroic mirror (Omega Optical, Inc.) was placed at the exit slits of the monochromator to remove the residual 355 nm light. The voltage signal was digitized by a digital oscilloscope (LeCroy LT374, 500 MHz, 4 gigasamples/s). The transient absorbance traces are the result of a single acquisition with no signal averaging over different laser shots.

Time-resolved difference absorbance spectra were measured using the on-axis exit port of the MS257 spectrograph, to which a gated intensified ccd (Andor Technology, iStar DH734, 1024 \times 1024 pixels) was coupled. The iccd was operated in the full vertical binning mode and the spectra were measured with a gating time of 3 ns. Spectra were measured in single shot fashion with 50 mJ, 355 nm laser pulses. Synchronization of the overall experiment (laser firing, shutter opening, and iccd triggering) was achieved by means of dedicated hardware.¹⁷

In the second setup,¹⁸ used for the studies with the pH indicators, monitoring at 633 nm was achieved by means of a HeNe laser (NEC Corporation). The cuvette (0.2 cm \times 1 cm) was held in a temperature-controlled sample holder (FLASH 100, Quantum Northwest, Inc.). The pump beam in this case was focused with a 0.5 m cylindrical lens: where it crossed the probe beam, its shape was an ellipsoid with minor axis 0.3 cm and major axis 1 cm. The transmitted intensity of the cw beam was monitored by a preamplified (Avtech AV149) avalanche silicon photodiode (Hamamatsu, S2382). A 0.25 m monochromator (H25, Jobin Yvon) was placed before the photodiode in order to remove stray light from the pump laser. The voltage signal was digitized by a digital sampling oscilloscope (LeCroy 9370, 1 GHz, 1 gigasample/s).

Data Analysis

Analysis of Photoacoustics Data. The sample waveform is assumed to be convolution of a reference waveform (determined with a compound releasing all of the absorbed energy as heat

(14) Barth, A.; Corrie, J. E. T. *Biophys. J.* **2002**, *83*, 2864–2871.

(15) Corrie, J. E. T. *J. Labelled Compd. Radiopharm.* **1996**, *38*, 403–410.

(16) Abbruzzetti, S.; Crema, E.; Masino, L.; Vecchi, A.; Viappiani, C.; Small, J. R.; Libertini, L. J.; Small, E. W. *Biophys. J.* **2000**, *78*, 405–415.

(17) Banderini, A.; Sottini, S.; Viappiani, C. *Rev. Sci. Instrum.* **2004**, *75*, 2257–2261.

(18) Abbruzzetti, S.; Viappiani, C.; Small, J. R.; Libertini, L. J.; Small, E. W. *J. Am. Chem. Soc.* **2001**, *123*, 6649–6653.

within a few nanoseconds) and a sum of exponential decay functions¹⁹

$$H(t) = \sum_i \frac{\varphi_i}{\tau_i} e^{-t/\tau_i} \quad (1)$$

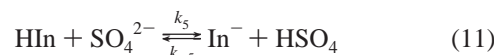
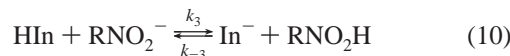
where φ_i is the pre-exponential factor of the transient with lifetime τ_i . The values of φ_i and τ_i are found from the deconvolution analysis.²⁰ We have determined the structural volume changes using a two-temperature method.²¹ The sample waveform was acquired at $T_{\beta=0}$ (3.9 °C in water²² and 2.7 °C in aqueous solutions with 0.1 M NaCl¹²) and was compared to a reference waveform acquired at a slightly higher temperature, $T_{\beta \neq 0} = 6.0$ °C. At $T_{\beta=0}$ the thermal expansion coefficient, β , is zero and the signals of thermal origin vanish. The sample waveforms measured at $T_{\beta=0}$ originate purely from structural changes in the solution and include no enthalpic contribution. The extent of the observed structural volume change for each decay component, ΔV_i , is calculated from φ_i as

$$\Delta V_i = \varphi_i E_\lambda \left(\frac{\beta}{C_p \rho} \right) \quad (2)$$

where E_λ is the molar energy content of the laser pulse, C_p the specific heat, and ρ the density. The thermoelastic parameter $\beta/C_p \rho$ is calculated at $T_{\beta=0}$. For dilute aqueous solutions and for pH values above 4, the thermoelastic parameter has essentially the same value as for water at pH 7 and can be determined from literature values,²² while for solutions with NaCl 0.1 M it must be determined experimentally using a comparative method.²³ When the reaction yield Φ_i is known, the reaction volumes $\Delta V_{R,i}$ can be determined from the equation

$$\Delta V_{R,i} = \frac{\Delta V_i}{\Phi_i} \quad (3)$$

Analysis of Data from Transient Absorbance. Transient 400 nm absorbance traces were analyzed with a sum of exponential decay functions and the data for proton-transfer reactions in the presence of the pH indicators were analyzed with a set of coupled differential equations. The chemical equilibria are derived from the proposed photolysis mechanism of caged sulfate shown in Scheme 1,¹⁴ and the ionic equilibria involving the pH indicators. The chemical equilibria relevant to the observed chemical relaxation are summarized below (CS = caged sulfate, RNO_2H is the nitronic acid **1**, and P is the nitrosoketone **4**)



It is assumed that photoexcitation leads to the formation of the nitronic acid RNO_2H with a particular yield within the duration of the laser pulse. This intermediate then partly deprotonates to give the *aci*-nitro anion RNO_2^- and a proton, and partly escapes to form the nitrosoketone **4** and the proton and sulfate products. The cyclic intermediate (**3** in Scheme 1) has not been explicitly considered since it does not appear to accumulate and therefore does not influence the observed kinetics.

In the above reaction scheme, protons are released in two steps, for which the relative amplitudes are determined by the pH that prevails immediately following the light flash. Results presented later in the paper show that at pH values well above the pK_a of the nitronic acid, full ionization occurs on the nanosecond time scale. When the pH is well below the pK_a , ionization of the nitronic acid is suppressed and proton release has a pH-dependent rate that is determined by decay of the nitronic acid to the final products. At pH values near the pK_a , the proton release partitions between these two pathways. Reactions 8, 10, and 11 influence the kinetics only to a minor extent and do not affect the overall equilibrium. At pH values close to or below neutrality, reactions with hydroxide ion were not included in the relevant equilibria because the very low concentration of this reactant means they make negligible contribution.

Results and Discussion

Transient 400 nm Absorbance as a Function of Pre-pulse pH. Figure 1 shows the absorbance changes at 400 nm of unbuffered aqueous solutions of caged sulfate at several initial pH values, following a single, 14 mJ laser pulse at 355 nm. The absorbance was observed to rise with a double exponential lifetime, $\tau_1 = 7 \pm 4$ ns and $\tau_2 = 63 \pm 6$ ns at pH 7. The first lifetime is at the limit of the experimental resolution of our apparatus and is ascribed to the formation of the nitronic acid **1**. The second transient is most likely associated with deprotonation of the nitronic acid to give the *aci*-nitro anion **2**, as suggested by studies on related compounds.^{11,24} Strong support for this assignment comes from the transient spectra shown in the right panel of Figure 1. The spectrum recorded at the end of the laser pulse is characterized by a band with a maximum at 396 nm, which can be attributed to the formation of **1**. At 100 ns delay, the absorbance increases and shifts to the red, with a peak at ~ 403 nm (suggesting the formation of **2**) and a

(19) Rudzki, J. E.; Goodman, J. L.; Peters, K. S. *J. Am. Chem. Soc.* **1985**, *107*, 7849–7854.

(20) Small, J. R. In *Numerical Computer Methods*; Brand, L., Johnson, M. L., Eds.; Academic Press: San Diego, 1992; Vol. 210, pp 505–521.

(21) Gensch, T.; Braslavsky, S. E. *J. Phys. Chem.* **1997**, *101*, 101–108.

(22) Weast, R. C., Ed. 52nd ed.; CRC Press: Boca Raton, 1971.

(23) Braslavsky, S. E.; Heibel, G. E. *Chem. Rev.* **1992**, *92*, 1381–1410.

(24) Il'ichev, Y. V.; Schwörer, M. A.; Wirz, J. *J. Am. Chem. Soc.* **2004**, *126*, 4581–4595.

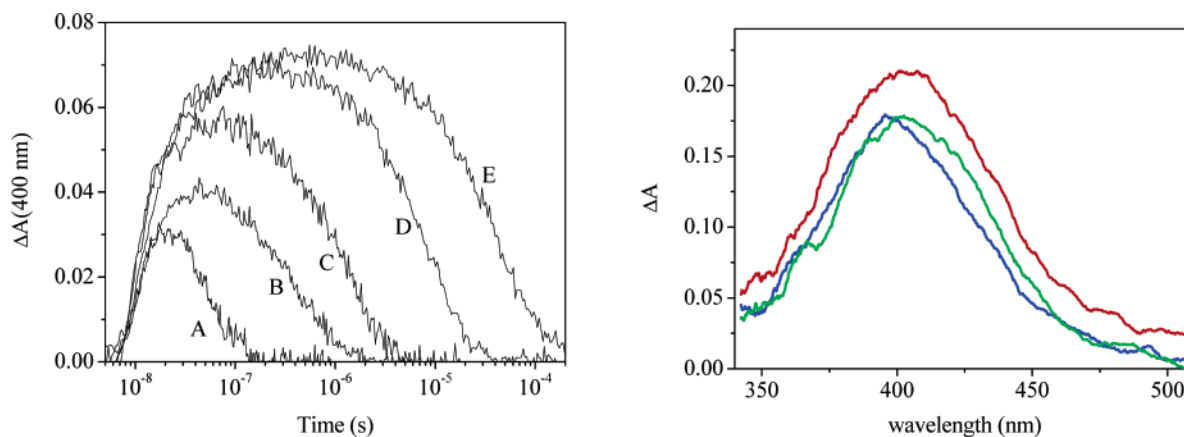


Figure 1. Left. Time courses of the transient absorbance traces at 400 nm for unbuffered aqueous solutions of 1 mM caged sulfate following a single, 14 mJ laser shot at 355 nm at several pH values. The initial pH values were: 1.6 (A), 2.5 (B), 3.1 (C), 4.1 (D), 6.8 (E). $T = 20\text{ }^{\circ}\text{C}$. Right. Single shot, transient absorbance spectra taken at the end of the laser pulse (blue curve), at 100 ns (red curve), and at 10 μs (green curve). The laser pulse energy was 50 mJ, $T = 20\text{ }^{\circ}\text{C}$, pre-pulse pH 7. The high laser energy used in this experiment leads to faster decay of the absorbance change at 400 nm than observed for curve E in the left panel (see text for a more detailed discussion of this effect).

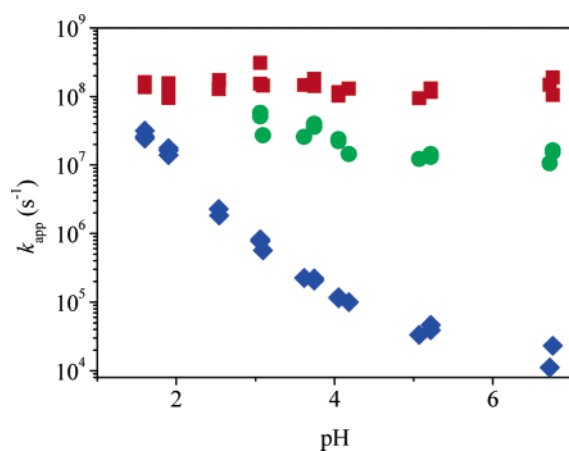


Figure 2. Rate constants for the formation (red squares, $k_{1,\text{app}}$; green circles, $k_{2,\text{app}}$) and decay (blue diamonds, $k_{3,\text{app}}$) of the 400 nm absorbance signal as a function of the initial pH of the solution. $T = 20\text{ }^{\circ}\text{C}$. The laser pulse energy was 14 mJ for all samples.

shoulder on the blue side, reflecting residual absorbance of the precursor **1**. As demonstrated by the data at 10 μs , the spectrum then decreases in amplitude with no change in shape, in parallel with the decay of **2**.

Decay of this absorbance was pH-dependent and the lifetime decreased from $\approx 100\text{ }\mu\text{s}$ at pH 7 to 34 ns at pH 1.6. Acid catalysis of this reaction is normally observed in other related systems²⁵ and has recently been discussed in terms of shifting the $\mathbf{1} \rightleftharpoons \mathbf{2}$ equilibrium to the left, so favoring formation of the bicyclic intermediate **3**.¹¹ Figure 2 reports the rate constants $k_{i,\text{app}} = 1/\tau_i$ at various pH values for these formation and decay processes. The slight increase in $k_{2,\text{app}}$ at acidic pH values is in agreement with the expected increase in relaxation rate for the equilibrium $\mathbf{1} \rightleftharpoons \mathbf{2}$ as the initial concentration of free protons is increased.

***Aci*-nitro Transient Absorbance as a Function of Laser Pulse Energy.** When studies were conducted in unbuffered solutions, the observed *aci*-nitro decay kinetics were dependent on the laser pulse energy used in the experiment. Appearance of the *aci*-nitro absorbance occurred with biexponential kinetics,

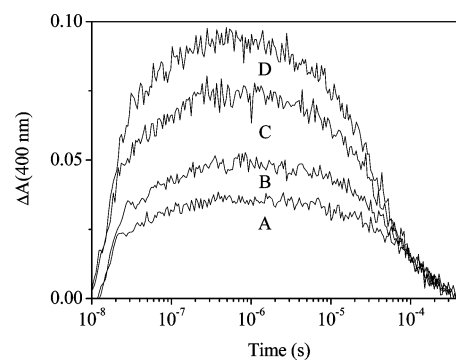


Figure 3. Time course of the transient absorbance at 400 nm for an unbuffered aqueous solution of 1 mM caged sulfate following a single 355 nm laser pulse at different laser pulse energies: A, 6 mJ; B, 10 mJ; C, 20 mJ; D, 30 mJ. The pre-pulse pH was 7.0. $T = 20\text{ }^{\circ}\text{C}$. Traces shown in the Figure are selected from several laser pulse energies investigated.

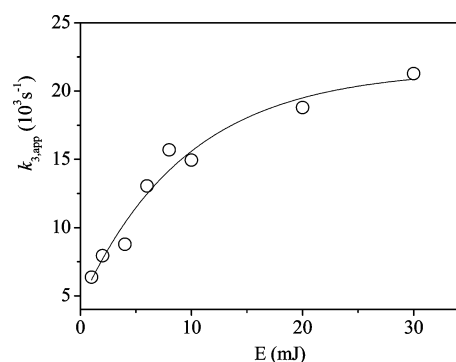


Figure 4. *Aci*-nitro decay rate ($k_{3,\text{app}} = 1/\tau_3$) as a function of laser pulse energy (between 1 mJ and 30 mJ). Pre-pulse pH 7.0, $T = 20\text{ }^{\circ}\text{C}$. The solid line is intended only to guide the eyes through the data points and has no kinetic meaning.

as described above, with lifetimes remaining fairly constant in the laser pulse energy range we have investigated ($\tau_1 = 7 \pm 4$ ns and $\tau_2 = 63 \pm 6$ ns). The *aci*-nitro absorbance decayed with a single-exponential relaxation, the rate of which increased with the laser pulse energy (Figures 3 and 4). Protons released by the nitronic acid accelerated the disappearance of the *aci*-nitro intermediate by an approximately 3-fold factor over the range of laser energies used. The effect was limited in these experiments because the photolysis laser beam was not focused, so

(25) McCray, J. A.; Trentham, D. R. *Annu. Rev. Biophys. Biophys. Chem.* **1989**, *18*, 239–270.

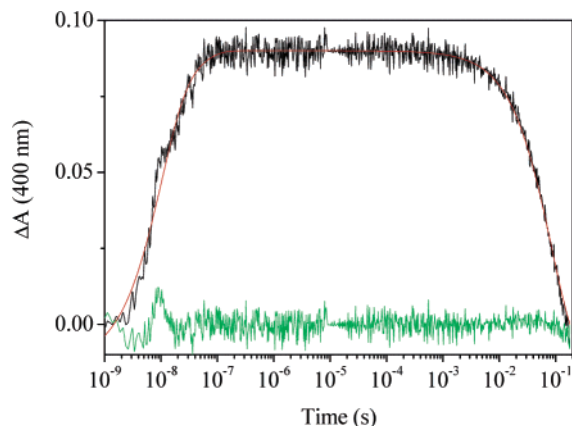


Figure 5. Transient absorbance at 400 nm (black trace) of a buffered (0.1 M HEPES, pH 7.0) aqueous solution of 1 mM caged sulfate. The red line overlapped to the black trace is the result of a fit with a triple exponential. Residuals of the fit are displayed as the green trace. $T = 20\text{ }^{\circ}\text{C}$.

the small extent of photolysis caused only minor pH changes. Larger effects of increased laser power were seen in the experiments with pH indicators, where the focused laser beam caused more extensive photolysis (see below).

The changes in $k_{3,\text{app}}$ observed with increasing laser pulse energy are much smaller than those observed when the pH is lowered below neutrality prior to photolysis (Figures 1 and 2). At the laser pulse energy (14 mJ) used in the experiments and at pre-pulse pH 6.8, shown in Figures 1 and 2, the *aci*-nitro decay rate is approximately $1.8 \times 10^4\text{ s}^{-1}$, a value which is almost unchanged until the pre-pulse pH is lowered below 5. This suggests that, at the photolysis level used in those experiments, the solution initially at pH 6.8 is lowered to \sim pH 5 when the equilibrium between **1** and **2** is established.

***Ac*-nitro Transient Absorbance in Buffered Solution.** The decay of the *aci*-nitro species is dramatically slowed in the presence of a buffer and a value of 34 s^{-1} at pH 7, $20\text{ }^{\circ}\text{C}$ was previously measured in 20 mM Mops buffer.¹⁴ Here, we measured the transient 400 nm absorbance at $20\text{ }^{\circ}\text{C}$ in 0.1 M HEPES buffer at pH 7. The absorbance increase is well described by two exponentials with lifetimes $9 \pm 1\text{ ns}$ and $36 \pm 9\text{ ns}$. The lifetime of the second process is noticeably shortened by the presence of the buffer. The decay is described by a single-exponential relaxation with lifetime $0.056 \pm 0.012\text{ s}$ (average of 4 determinations), corresponding to a rate constant of $18 \pm 4\text{ s}^{-1}$. A representative signal is shown in Figure 5 along with a fit and the corresponding residuals plot. An inverse relationship between ionic strength and *aci*-nitro decay rates has previously been reported in a detailed mechanistic study on the photolysis of caged ATP.²⁵

It is possible to identify the deprotonation kinetics of the nitronic acid **1** in the slower transient of the rising phase of the 400 nm absorbance data. In unbuffered neutral solutions this ionization has a lifetime of $63 \pm 6\text{ ns}$, corresponding to a deprotonation rate $k_2 \approx k_{2,\text{app}} = (1.58 \pm 0.09) \times 10^7\text{ s}^{-1}$. Assuming for the protonation rate a diffusion-limited value, i.e., $\sim 5 \times 10^{10}\text{ M}^{-1}\text{ s}^{-1}$,³ the $\text{p}K_{\text{a}}$ of the acid intermediate can be estimated [from $-\log(k_{2,\text{app}}/k_2)$] as 3.5 ± 0.2 . By comparison, Wirz and co-workers recently reported a deprotonation rate of $(2.7 \pm 0.3) \times 10^6\text{ s}^{-1}$ (lifetime $\sim 370\text{ ns}$) for 2-nitrobenzyl methyl ether, corresponding to a $\text{p}K_{\text{a}}$ of 4.3.²⁴ Deprotonation of the nitronic acid formed after photoexcitation of the parent

Table 1. Comparison of Lifetimes for the Deprotonation of the Nitronic Acid at Pre-pulse pH 7

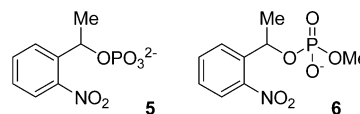
caged species	τ_2 (ns)	$k_{2,\text{app}}$ (10^7 s^{-1})	$\text{p}K_{\text{a}}^a$
sulfate	63 ± 6	1.58 ± 0.09	3.76 ± 0.06
methyl phosphate	78 ± 16	1.28 ± 0.26	3.84 ± 0.2
phosphate	270 ± 58	0.37 ± 0.08	4.39 ± 0.22

^a On the basis of $k_2 = 9 \times 10^{10}\text{ M}^{-1}\text{ s}^{-1}$, as suggested by the data on caged sulfate, see Table 2.

compound 2-nitrotoluene was reported to occur with rate $2 \times 10^7\text{ s}^{-1}$.¹¹ A better estimate of the $\text{p}K_{\text{a}}$ of the acid intermediate **1** is given in a following section.

The $\text{p}K_{\text{a}}$ value of the nitronic acid means that it is completely deprotonated at pre-pulse pH values >4.5 . Below this pH, an increasing proportion of the protons is trapped on the nitronic acid and a second deprotonation event occurs when sulfate is released, thus giving rise to a second, much slower proton release process. This mechanism is confirmed by the studies with pH indicators reported below.

The information on the $\text{p}K_{\text{a}}$ of the nitronic acid **1** and gradual emergence of corresponding data for related nitronic acids (vide supra) stimulated us to examine the deprotonation of nitronic acids from two related compounds, caged phosphate **5** and its monomethyl ester (caged methyl phosphate **6**). We anticipated that the nitronic acids from caged sulfate and caged methyl phosphate would have similar acidities, but that the nitronic acid from caged phosphate would be a weaker acid because of the presence of two negative charges on the phosphate. Photolysis of neutral aqueous solutions of these compounds leads to a biphasic increase in absorbance at 400 nm, with a fast phase at the limit of the experimental resolution ($\sim 7\text{ ns}$), followed by a second, slower transient. The lifetimes of the second phase for the three compounds, corresponding to the deprotonation of the nitronic acids, are compared in Table 1. While caged methyl phosphate and caged sulfate are characterized by similar lifetimes, deprotonation of the nitronic acid for caged phosphate occurs with a significantly longer lifetime. The derived $\text{p}K_{\text{a}}$ estimates for the nitronic acids thus afford similar values for caged sulfate and caged methyl phosphate, while the nitronic acid from caged phosphate is clearly a weaker acid (Table 1). The variation of acidity between different nitronic acids must be a factor in determining different *aci*-nitro decay kinetics for different caged compounds, since it will affect the position of the equilibrium between the nitronic acid and its related *aci*-nitro anion, and hence will influence the rate of escape from the *aci*-nitro anion to the bicyclic species **3** and onward to product release.^{11,26}

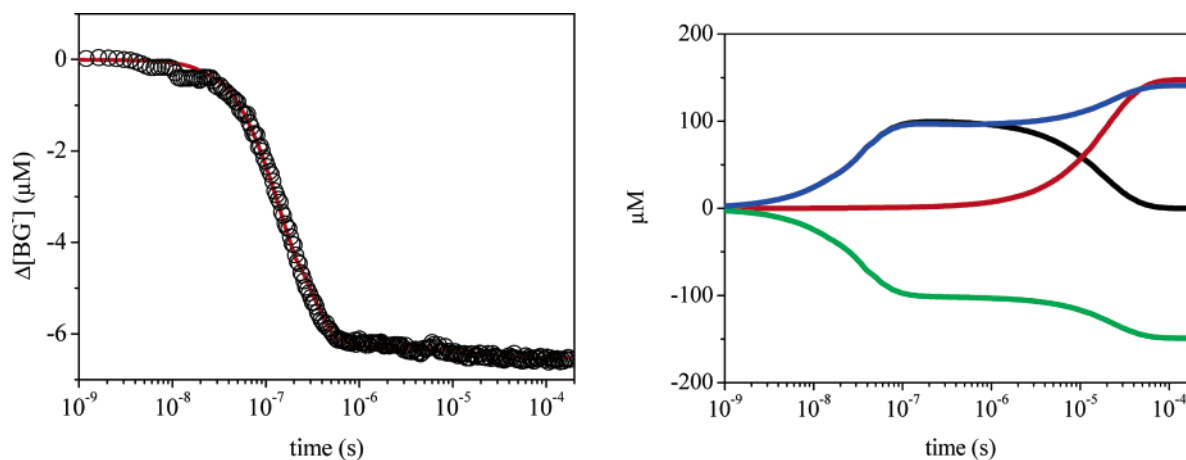


Kinetic Investigations with pH Indicators. The photoinduced proton release processes from caged sulfate can be further understood by studying proton-transfer reactions with suitable pH indicators. In these experiments, the combination of a focused laser pulse and higher concentration of caged sulfate means that much more photolysis took place than in the

(26) Il'ichev, Y. V.; Wirz, J. *J. Phys. Chem. A* **2000**, *104*, 7856–7870.

Table 2. Parameters Determined from the Numerical Fitting of the Time Courses of the Concentration Changes of the pH Indicators Using the Differential Equations Associated with Reactions 4–11

reaction	fitted parameters	rate constants
$\text{H}^+ + \text{In}^- \rightarrow \text{HIn}$	k_1	$(6.09 \pm 0.06) \times 10^{10} \text{ M}^{-1} \text{ s}^{-1}$ (BG) $(5.17 \pm 0.05) \times 10^{10} \text{ M}^{-1} \text{ s}^{-1}$ (BB)
$\text{H}^+ + \text{R-NO}_2^- \rightarrow \text{R-NO}_2\text{H}$	k_2	$(9.15 \pm 0.05) \times 10^{10} \text{ M}^{-1} \text{ s}^{-1}$
$\text{R-NO}_2\text{H} \rightarrow \text{H}^+ + \text{R-NO}_2^-$	k_{-2}	$(1.8 \pm 0.2) \times 10^7 \text{ s}^{-1}$
$\text{HIn} + \text{RNO}_2^- \rightarrow \text{In}^- + \text{RNO}_2\text{H}$	k_3	$(2.66 \pm 0.01) \times 10^7 \text{ M}^{-1} \text{ s}^{-1}$ (BG)
$\text{R-NO}_2\text{H} \rightarrow \text{R-SO}_3\text{H}$	k_4	$(1.45 \pm 0.04) \times 10^5 \text{ s}^{-1}$
$\text{HIn} + \text{SO}_4^{2-} \rightarrow \text{In}^- + \text{HSO}_4^-$	k_5	$(5.3 \pm 0.1) \times 10^6 \text{ M}^{-1} \text{ s}^{-1}$ (BG)
$\text{RNO}_2\text{H} + \text{SO}_4^{2-} \rightarrow \text{RNO}_2^- + \text{HSO}_4^-$	k_6	$(5.3 \pm 0.1) \times 10^6 \text{ M}^{-1} \text{ s}^{-1}$
pK_a nitronic acid		3.69 ± 0.05
pK_a sulfate group		1.8 ± 0.1

**Figure 6.** Left. Changes in concentration of BG^- (circles) after flash photolysis of an unbuffered solution containing 4 mM caged sulfate. Pre-pulse pH was 7, $T = 20^\circ \text{C}$. The laser pulse energy was 20 mJ. The red solid curve is the result of the fit using the set of equations derived from equilibria 4–11. Right. Time profile of the concentration changes of nitronic acid (green line), *aci*-nitro anion (black line), protons (blue line) and free sulfate (red line) resulting from the numerical solutions of the differential equations.

experiments reported above. We used two different pH indicators, bromocresol green (BG), with pK_a 4.9 and bromophenol blue (BB), with pK_a 4.1.²⁷ Both indicators show a strong absorbance band in the red, which decreases toward zero as the indicators are titrated through and below their pK_a . Acidification of the solution can therefore be followed easily in the visible region (here at 633 nm) through changes in relative concentrations of deprotonated and protonated indicator species. The advantage of this approach is that the kinetics of the changes in concentration of deprotonated indicator reflect all of the equilibria [eqs 1–8] and can be used to understand how the chemical equilibria interact to produce the observed kinetics. Most importantly, we can characterize the kinetics of proton release from caged sulfate.

Numerical solutions to the set of coupled differential equations corresponding to equilibria 4–11 were determined by using the function ODE15s within Matlab 6.1 (The MathWorks, Inc.). The numerical solution of the set of equations depends on several rate constants and concentrations which were considered as fitting parameters, that can be optimized using a nonlinear fitting algorithm. For this, we used a Matlab version of the optimization package Minuit (CERN). To improve the quality and reliability of the retrieved parameters, we have chosen to leave only some of them as free parameters to be optimized and to use global analysis of curves taken under different experimental conditions, namely pre-pulse pH, laser pulse

energy, and pH indicator. Depending on the combination of curves, some of the parameters were left free to vary from curve to curve and others were constrained to have the same value for all of the curves. Table 2 summarizes the most relevant parameters we have obtained from the analysis. Backward rate constants were calculated from pK_a values and the corresponding forward rate constants.

When the solution containing caged sulfate and the pH indicator (either BG or BB) is flashed, a rapid decrease in 633 nm absorbance is observed, associated with protonation of the indicator. The change in absorbance is converted to change in concentration upon division by the molar extinction coefficient of the deprotonated indicators at 633 nm, i.e., $33\,000 \text{ M}^{-1}\text{cm}^{-1}$ for BG,⁷ and $70\,000 \text{ M}^{-1}\text{cm}^{-1}$ for BB (this work), respectively. Figure 6 shows a typical result of the fit to a transient absorbance trace measured for BG following flash photolysis of caged sulfate. In this Figure we show a sample curve from a global analysis conducted on traces measured at several laser pulse energies with the same pre-pulse pH. From the protonation kinetic curve it is evident that binding occurs mainly with a rate in the 10^7 s^{-1} range. The observed rate is consistent with the value expected for a diffusion controlled reaction (with bimolecular rate $\sim 5 \times 10^{10} \text{ M}^{-1} \text{ s}^{-1}$), corresponding to $\sim 0.5 \times 10^7 \text{ s}^{-1}$ at a concentration of $100 \mu\text{M}$ photoreleased protons. This process occurs when protons released by the nitronic acid bind to the pH indicator. However, a minor decrease in BG^- is observed on the 10^{-5} s time scale, showing that some additional protons become available on this time scale. The kinetic model

(27) Bishop, E. *Indicators*; Pergamon Press: Oxford, 1972.

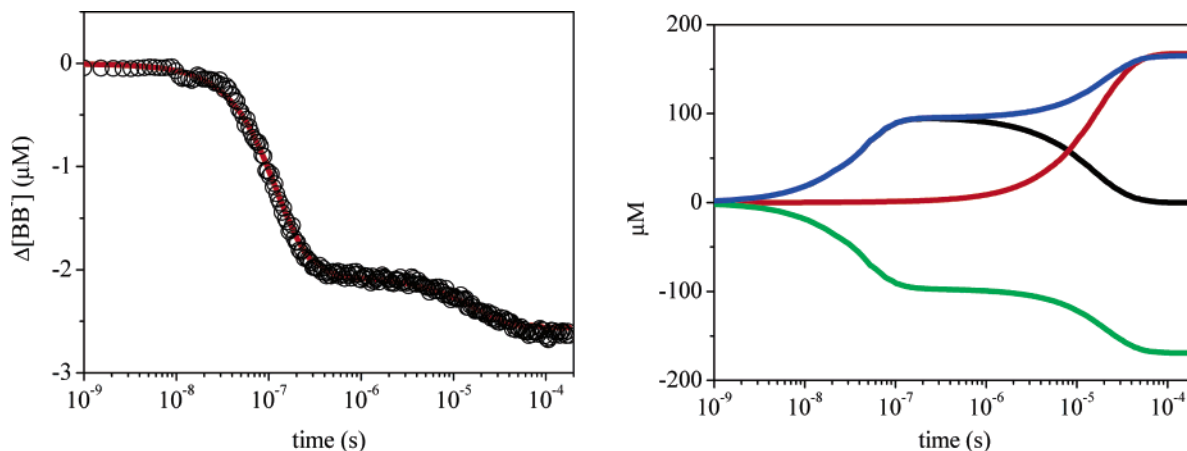


Figure 7. Left. Changes in concentration of BB⁻ (circles) after flash photolysis of an unbuffered solution containing 4 mM caged sulfate. Pre-pulse pH was 7, $T = 20$ °C. The laser pulse energy was 20 mJ. The red solid curve is the result of the fit using the set of equations derived from equilibria 4–11. Right. Time profile of the concentration changes of nitronic acid (green line), aci-nitro anion (black line), protons (blue line) and free sulfate (red line) resulting from the numerical solutions of the differential equations.

derived from eqs 4–11 readily attributes this second step to the release of protons when the sulfate group is released. The first step (release from the nitronic acid) accounts for a fraction of the total released protons. The deprotonation yield of the nitronic acid that is <1 and the low release rate ($\sim 1.25 \times 10^7$ s⁻¹) both arise from the relatively high pK_a of intermediate **1**. Experiments were repeated at several values of the pre-pulse pH between 7 and 4.5 and a global analysis of these data showed that the set of differential equations satisfactorily reproduced all conditions (data not shown).

The slower deprotonation step becomes much more evident when BB is used to sense the photoreleased protons as the lower pK_a of this indicator provides higher sensitivity to observe the second phase of deprotonation. This property is strikingly evident in Figure 7, where a large step on the 10 μs time scale is clearly discernible from the concentration change of BB⁻. Figure 7 shows also the result of the fit to the transient absorbance trace measured for BB following photolysis of caged sulfate. The Figure reports a sample curve out of a global analysis conducted on traces measured at several laser pulse energies with the same pre-pulse pH. Other conditions were the same as for the BG experiments.

Figure 8 compares the proton release kinetics corresponding to increasing laser pulse energy. It is clear that the slower phase becomes more prominent as the laser pulse energy is increased. This effect can be rationalized by considering that as the laser pulse energy is increased, a larger concentration of nitronic acid is formed. Proton release from the nitronic acid lowers the pH and so suppresses its ionization, thus blocking a proportion of the ionizable protons on the nitronic acid itself. This negative feedback is not expected to be effective at low laser pulse energy (as in the experiments reported in Figure 1), since the concentration of protons released by the nitronic acid is not sufficiently high to lower the pH below 4.5 and shift the equilibrium between **1** and **2** significantly to the left.

The value of k_2 in Table 2 is on the high side for protonation reactions of a weak oxygen base, likely reflecting the presence of the additional negative charge of the sulfate, as previously observed for sulfonated derivatives of hydroxypyrene and naphthols.⁶ Using k_2 from Table 2, and the apparent rate constant $k_{2,app}$ ($\sim k_2$) = $(1.58 \pm 0.09) \times 10^7$ s⁻¹ we can estimate the pK_a

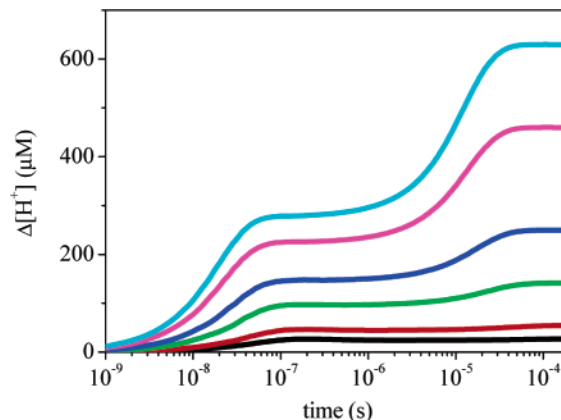


Figure 8. Time profile of the proton concentration change at several values of laser pulse energy (black: 6 mJ; red: 10 mJ; green: 20 mJ; blue: 40 mJ; magenta: 80 mJ; cyan: 120 mJ). The curves were generated by integration of the differential equations corresponding to equilibria 4–11.

as 3.76 ± 0.06 (Table 1), which is in line with the value reported in Table 2 that was obtained from the numerical analysis. Given the large error bar, the value of k_{-2} in Table 2 is consistent with $k_{2,app}$, although slightly larger.

Time-Resolved Photoacoustics

The photoacoustic signals measured for aqueous solutions of caged sulfate at $T = T_{\beta=0}$ at pH values below neutrality are best described by double exponential kinetics with negative pre-exponential factors, which show that photoexcitation leads to a contraction of the solution. Figure 9 shows representative photoacoustics data measured at pH 2.2 together with the fit to a double exponential decay.

Reasonably good fits were obtained at all pH values with double exponential decays, although around pH 3.5 triple exponential kinetics led to some improvement of the analysis. However, given the very close values of the lifetimes, the retrieved parameters are in some cases unstable. This is evident from the volume changes associated with processes 1 and 2 in Figure 10, right panel, showing a very noisy pH dependence at $pH \approx 3.5$. In general, the lifetimes of transients 2 and 3 are pH dependent, and increase with pH (Figure 10, left panel). The lifetime of process 2 reaches a plateau value of ~ 40 ns at pH

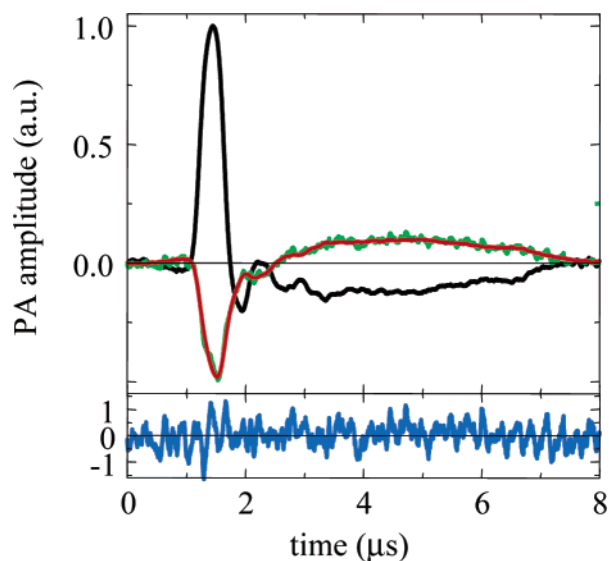


Figure 9. Deconvolution analysis for volumetric signals measured at pH 2.2. Reference signal (black curve) was measured at 6 °C, volumetric signal (green curve) was measured at 2.7 °C. Best fit is shown as the red line overlapped to the green curve and was obtained with double exponential kinetics. Residuals are displayed in blue on an expanded y-scale ($\times 10$).

> 4 . At pH < 3.5 the lifetime of transient 2 becomes too short to be resolved and merges into the fast component with sub-resolution lifetime. The lifetime of the intermediate 3 increases above the upper limit of the experimental resolution ($\approx 10 \mu\text{s}$) when the pH is increased to values higher than 4. The corresponding amplitudes, reported in the left panel of Figure 10, suggest that these transients reflect the ionization equilibria for the associated reactions.

The identity of the observed transients can be inferred using the transient absorbance data reported above and using the volume changes previously determined for photoinduced processes in other 2-nitrobenzyl compounds. Transient 1 is accompanied by a contraction of the solution and has a lifetime below the experimental resolution (~ 10 ns). Correspondingly, a fast component in the rise of the 400 nm absorbance signal (with lifetime of ~ 7 ns, i.e., at the limit of the experimental resolution) is observed at all investigated pH values. These features suggest that the process of transient 1 is rapid formation of the nitronic acid (**1** in Scheme 1), which is known to occur on subnanosecond time scale in other 2-nitrobenzyl compounds.^{28–30} The more polar character of the nitronic acid **1** with respect to the parent compound is responsible for the observed contraction of the solution.³¹

The lifetime of process 2 is very similar to that of the second component in the rising part of the transient absorbance (Figure 11). The slightly higher rate may be an artifact due to the close values of two faster transients, which are difficult to separate in the photoacoustic experiment. This process is accompanied by a contraction, whose amplitude decreases as the pH is decreased below ~ 3.5 , showing that this transient is associated with deprotonation of the nitronic acid **1** to give the nitronate

anion **2**. The volume change associated with deprotonation of the nitronic acid (**1** \rightarrow **2** in Scheme 1, process 2) should give rise to pH-dependence characterized by a sigmoidal shape. However, given the lifetime of this process, it is very difficult precisely to retrieve the amplitude of the associated volume change and the resulting trend of this parameter is partly mixed with the fast, pH-independent process 1. Figure 10 reports the result of the fit to the volume changes associated with process 2 using the Henderson–Hasselbach model. The best fit was obtained with $\text{p}K_{\text{a}} = 3.7 \pm 0.2$, in very good agreement with the value obtained from the analysis of the protonation kinetics of the pH indicators.

The lifetime of process 3 is in excellent agreement with that obtained from the absorbance change due to the *aci*-nitro decay **1** \rightarrow **3** (Figure 11). A clear pH dependence for the amplitude of process 3 is discernible from Figure 10. Unfortunately, the lifetime of the transient at pH above 3.5 becomes too long to be detected by the photoacoustic setup and only part of the associated curve can be drawn precisely. This hinders the ability to retrieve reliable equilibrium parameters for this process. This reaction leads to release of the sulfate and a solvated proton and is expected to give rise to a very large contraction of the aqueous solution, since the reaction volume for deprotonation of HSO_4^- at 25 °C is -21.2 mL/mol .³² Although the overall reaction we are observing is not simply an analogue of the deprotonation of HSO_4^- , the net effect on the reaction volume is expected to be similar, since the neutral nitrosoketone byproduct **4** should have a minimal solvation signal. Indeed, a large contraction ($\sim -6 \text{ mL/mol}$) is measured at pH 3.5.

The contribution by process 3 decreases as the pH is raised above 3.5, since the nitronic acid is almost completely deprotonated at pH above 4. Therefore, proton release is essentially complete after the nitronic acid has completed the ns processes. Above these pH values, sulfate release is not accompanied by a further acidification of the solution, and the volume change is essentially due to the difference in molar volume between the nitronate anion and the solvated sulfate.

We have previously shown that time-resolved photoacoustics experiments at alkaline pH allow the determination of deprotonation yields for 2-nitrobenzaldehydes.^{8,13,33} When the pH is raised above neutrality, the fast contractions observed upon excitation of caged sulfate at acidic pH are followed by an expansion, the lifetime of which decreases at increasing pH values. This expansion is associated with the bimolecular neutralization reaction of hydroxide. In the alkaline pH range, the concentration of hydroxide is in large excess with respect to the concentration of photodetached protons, normally below $1 \mu\text{M}$ at the laser pulse energy used in the photoacoustics experiments. This results in pseudo-first-order kinetics. The measured expansion has a value of $\Delta V_2 = 6.3 \pm 0.4 \text{ mL/mol}$ in the pH range 9–11. Using the known value of the reaction volume for water formation $\Delta V_{\text{W}} = 22.84 \text{ mL/mol}$,^{31,34} we can determine the quantum yield for the deprotonation reaction $\Phi_{\text{H}^+} = \Delta V_2/\Delta V_{\text{W}} = 0.28 \pm 0.02$. This quantum yield estimate is smaller by an almost 2-fold factor when compared with a previous determination (0.47).¹⁴ The disagreement can be

(28) Yip, R. W.; Sharma, D. K.; Giasson, R.; Gravel, D. *J. Phys. Chem.* **1984**, *88*, 5770–5772.

(29) Yip, R. W.; Sharma, D. K.; Giasson, R.; Gravel, D. *J. Phys. Chem.* **1985**, *89*, 5328–5330.

(30) Yip, R. W.; Wen, Y. X.; Gravel, D.; Giasson, R.; Sharma, D. K. *J. Phys. Chem.* **1991**, *95*, 6078–6081.

(31) VanEldick, R.; Asano, T.; LeNoble, W. J. *Chem. Rev.* **1989**, *89*, 549–688.

(32) Larson, J. W.; Zeeb, K. G.; Hepler, L. G. *Can. J. Chem.* **1982**, *60*, 2141–2150.

(33) Bonetti, G.; Vecchi, A.; Viappiani, C. *Chem. Phys. Lett.* **1997**, *269*, 268–273.

(34) Asano, T.; Noble, W. J. L. *Chem. Rev.* **1978**, *78*, 407–489.

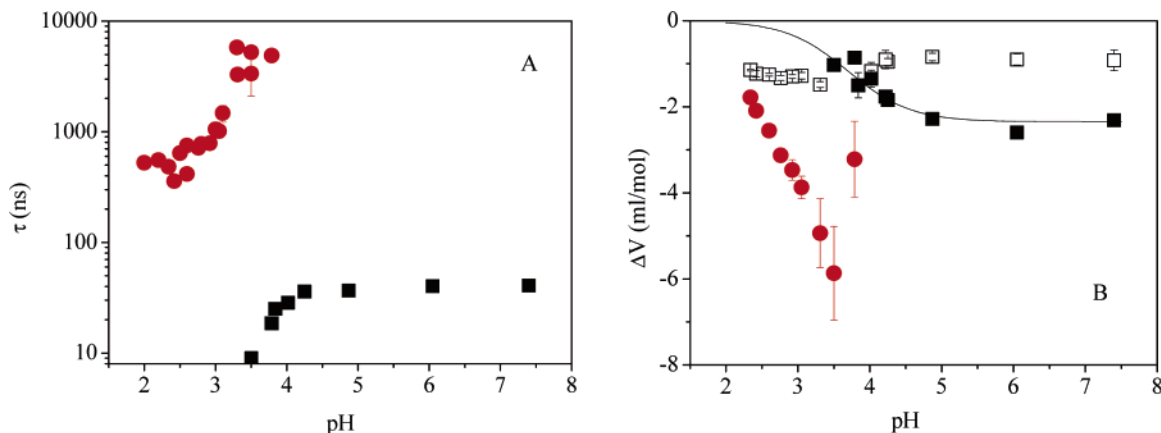


Figure 10. Lifetimes (left) and observed volume changes (right) associated with the transients detected by time-resolved photoacoustics as a function of pH below neutrality. Open squares refer to process 1, filled squares process 2, filled red circles, process 3. $T = 2.7$ °C. $[\text{NaCl}] = 0.1$ M. The solid line is the result of a fit with a Henderson-Hasselbach model to the volume changes associated with process 2.

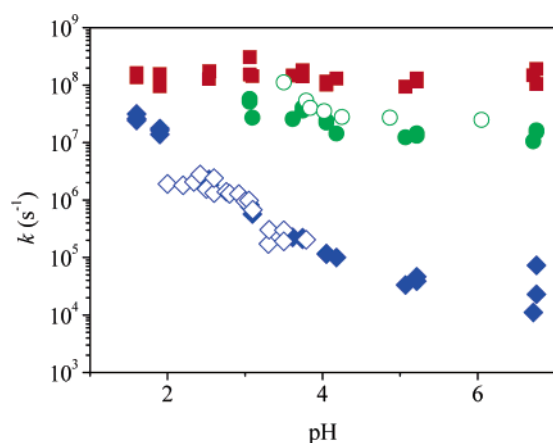


Figure 11. Comparison of the rate constants determined with time-resolved photoacoustics (open symbols) and laser flash photolysis (filled symbols). Red squares, process 1, green circles, process 2, blue diamonds, process 3. The smaller temporal range that can be spanned by time-resolved photoacoustics allows comparisons only over limited portions of the investigated pH range.

rationalized by considering the limited capability of photoacoustics methods in retrieving correct amplitudes for processes characterized by close values of lifetimes. In the system under investigation, the lifetime of the short-lived transients 1 and 2 are very close to each other and, at pH above 10, they also overlap the reaction of released protons with hydroxide. Under these conditions, the three processes are not resolved and a nanosecond contraction due to formation of the nitronic acid is followed by an expansion, likely containing the volume changes associated both with proton release by the nitronic acid and the neutralization of hydroxide. The apparent rate constant for this expansion is plotted in Figure 13 as a function of the concentration of free hydroxide. It is clear that the measured rate does not reflect a simple pseudo-first-order bimolecular process, for which a straight line with slope $\sim 5 \times 10^{10} \text{ M}^{-1} \text{ s}^{-1}$ should be obtained. On the contrary, the apparent rate constants reach a plateau value of $\sim 1.5 \times 10^7 \text{ s}^{-1}$ as the $[\text{OH}^-]$ is increased, corresponding to a lifetime of ~ 70 ns. The value is the same as that determined for deprotonation of the nitronic acid. This finding can be rationalized by considering the deprotonation to act as a rate-limiting step for the subsequent protonation of

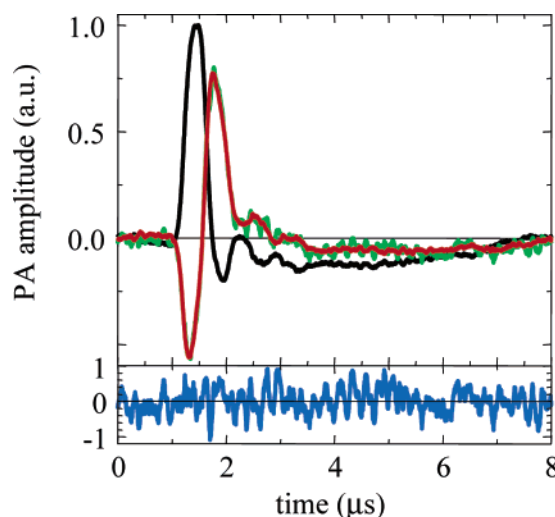


Figure 12. Deconvolution analysis for volumetric signals measured at pH 10.5. Reference signal (black curve) was measured at 6 °C, volumetric signal (green curve) was measured at 2.7 °C. Best fit is shown as the red line overlapped with the green curve and was obtained with double exponential kinetics. Residuals are displayed as the blue curve on an expanded y-scale ($\times 10$).

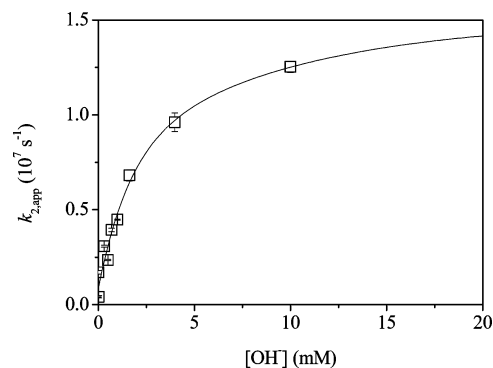


Figure 13. Apparent rate constant estimated from photoacoustic measurements for the neutralization of hydroxide by photoreleased protons as a function of $[\text{OH}^-]$. The saturating rate was estimated as the asymptotic value at very high $[\text{OH}^-]$, retrieved from the curve (black solid line) that is fitted to a double exponential.

hydroxide. The apparent rate constant in the presence of excess hydroxide is therefore the proton release rate.

Conclusions

Deprotonation of caged sulfate induced by nanosecond laser photolysis at 355 nm occurs on the ~ 100 nanosecond time scale at neutral pH. The deprotonation rate is determined by the pK_a of the nitronic acid intermediate **1**, and measurement of the rates for two related compounds gives some insight on factors that influence these pK_a values. At acidic pre-pulse pH, deprotonation of the nitronic acid is not complete and a proportion of the ionizable protons remains on the nitronic acid itself. These protons are released on the microsecond time scale, concomitant with the decay of **1**, with a rate determined by the pre-pulse pH of the solution.

When caged sulfate is used to induce large changes in free proton concentration, ionization of the nitronic acid **1** acts as a negative feedback on further proton liberation and increases the proportion of proton release that takes place in a slower, microsecond phase. However, even at the largest change in free proton concentration we could achieve ($\sim 600 \mu\text{M}$), there is no interference of the sulfate product with the release kinetics. The absence of buffering by the sulfate product is a principal advantage of the compound. This property makes it possible to reach pH values which, for example, can cause full acid denaturation of myoglobin.¹⁴ However, the relatively long time scale of proton release (μs) when very acidic pH-jumps are induced means that the compound will have limited applicability for study of low pH processes with lifetimes shorter than $\sim 10^{-4}$ s. This issue might be addressed by other caged sulfate reagents

that can be envisaged, based on the 3',5'-dimethoxybenzoic or *p*-hydroxyphenacyl cages.^{35–39} These have the potential to release protons in a single phase on a fast (ns) time scale. However, both these chromophores have lower absorption coefficients in the 350 nm region than NPE-caged sulfate, so may be less able to achieve the large pH jumps that are accessible with the present reagent. It is likely that no single reagent will be able to fulfill all possible requirements for laser-induced proton jumps but the present caged sulfate is nevertheless an advance on previous compounds used for this purpose.

Acknowledgment. C.V. acknowledges INFM and MIUR (FIRB Nanotechnologies, COFIN2001) for financial support. We are grateful to Dr Ranjit Munasinghe for technical support with preparation of caged sulfate.

Supporting Information Available: Absorbance spectra of caged sulfate, bromocresol green, and bromophenol blue. This material is available free of charge via the Internet at <http://pubs.acs.org>.

JA051702X

- (35) Corrie, J. E. T.; Trentham, D. R. *J. Chem. Soc., Perkin Trans. 1* **1992**, *1*, 2409–2417.
- (36) Thirlwell, H.; Corrie, J. E. T.; Reid, G. P.; Trentham, D. R.; Ferenczi, M. A. *Biophys. J.* **1994**, *67*, 2436–2447.
- (37) Shi, Y.; Corrie, J. E. T.; Wan, P. J. *Org. Chem.* **1997**, *62*, 8278–8279.
- (38) Givens, R. S.; Jung, A.; Park, C.; Weber, J.; Bartlett, W. *J. Am. Chem. Soc.* **1997**, *119*, 8369–8370.
- (39) Conrad, P. G.; Givens, R. S.; Hellrung, B.; Rajesh, C. S.; Ramseier, M.; Wirz, J. *J. Am. Chem. Soc.* **2000**, *122*, 9346–9347.